Electronic supplementary information (ESI)

3D hierarchical assembly of optimized heterogeneous carbon nanosheets for highly efficient electrocatalysis

*Gang Wan[a,b], Ming Ma[a,b], Alec(Yi) Jia[b], Lisong Chen[a,b], Yu Chen[a,b], Xiangzhi Cui[a,b], Hangrong Chen[a,b] *, Jianlin Shi[a,b]*

[a]State Key Laboratory of High Performance Ceramics and Superfine Microstructures, Shanghai Institute of Ceramics, Chinese Academy of Sciences, 1295 Ding-xi Road, Shanghai 200050 (P. R. China), Fax: (+86) 21-5241-312

[b]University of Chinese Academy of Sciences, Beijing 100049

[c]Queensland Micro- and Nanotechnology Centre(N44) 3.08, Nathan campus, Griffith University, Nathan, Queensland 4111, Australia, Tel: (07) 373 55057

Part A: Experimental section

Materials:

The 8-hydroxyquinoline and iron chloride hexahydrate were purchased from J&K Chemicals, 40% Pt/C was provided by Sigma Aldrich coorporation.

The synthesis of the catalysts

Firstly, 0.006 mol 8-hydroxyquinoline was dissolved in 40 ml ethanol in beaker A, and 0.002 mol ferric chloride was dissolved in 10 ml deionized water in beaker B, then the solution of beaker B was added into beaker A, followed by magnetic stirring in darkness for 6 h. After centrifugalization and washed with deionized water twice, the

obtained 8-hydroxyquinoline iron complex compounds were freeze-dried and then mixed with additional 8-hydroxyquinoline in the mass ratio 1:3 with fine grind in an agate mortar. The obtained materials were subjected to heat treatment with 10 °C min^{-1} temperature ramp rate under the nitrogen condition for 2 h pyrolyzation time at 800 °C. The pyrolyzed materials were leached in 3 mol/L hydrochloric acid at 80°C for 8 hours, followed by washing with deionized water until the neutral pH and freeze-dried. The final catalyst 3D-Fe-N-CNS-N was obtained after fine grinding. And catalysts 3D-Fe-N-CNS-N-1 and 3D-Fe-N-CNS-N-2 were prepared with the additional 8-hydroxyquinoline in the mass ratio 1:1 and 1:2 respectively. 3D-Fe-N-CNS was prepared following the same process by pyrolyzing the obtained 8-hydroxyquinoline iron complex compounds without adding the additional 8-hydroxyquinoline.The 8-hydroxyquinoline with a low melting point of 75°C easily sublimated during the pyrolysis process, leading to further nitrogen doping.

Physical characterization

The transition electron microscopy (TEM) images in this work were collected from a JEOL-2010F electron microscope operated at 200 kV. The field-emission scanning electron microscopy (FE-SEM) images were obtained on a Hitachi S-4800 scanning electron microscope. The powder X-ray diffraction (XRD) patterns of the as prepared samples were recorded on a Rigaku D/Max-2550 V X-ray diffractometer with a Cu Kα radiation target (40 KV, 40 mA), and the scanning rate was 4°per minute. X-ray photoelectron spectroscopy (XPS) signals were collected on a VG Micro MK II instrument using monochromatic Mg Ka X-rays at 1253.6 eV operated at 150 W, and

spectrum calibration was performed by taking the C 1s electron peak (BE = 285 eV) as internal reference. The nitrogen adsorption-desorption measurement was performed using Micromeritics Tristar 3000 at 77 K, and the specific surface area and pore size distribution were calculated using the Brunauer-Emmett-Teller (BET) and Barrett-Joyner-Halenda (BJH) methods, respectively. Inductively Coupled Plasma–Atomic Emission Spectrometer (ICP-AES) was conducted in SHIMADZU ICPS-8100. The samples for ICP-AES analysis was first heated at 700 ^{o}C for 2 h in air, followed by treatment in aqua regia.

Electrocatalytic activity evaluation

All the electrochemical measurements were carried out on CHI 760E electrochemical workstation (CH Instrument, Inc.) with a standard three-electrode cell at room temperature.A platinum wire and Ag/AgCl (3 MKCl) were used as counter and reference electrodes, respectively. And the Ag/AgCl potentials are converted to RHE using the following Nernst equation: $E_{RHE}=E_{Ag/AgCl}+0.209+0.059PH$

a.) A glass carbon disk (GCE, 6 mm diameter) and a Rotating ring-disk electrode (RRDE) with a Pt ring (4 mm inner-diameter and 6 mm outer diameter) severed as the substrate for the working electrode for evaluating the ORR activity and selectivity of various catalysts. Prior to use, glassy carbon electrode was polished alumina slurry (1.0 μm, 0.3 μm and 0.05 μm) in sequence, and ultrasonically cleaned thoroughly with pure water between each polishing step.Catalyst ink was prepared by blending catalyst power (10 mg) with 2 mL of mixed solution (ethanol:water = 1 : 1, volume scale) and 50μL Nafion solution (5%) in the ultrasonic bath.

b.) For cyclic voltammetry (CV) and rotating ring-disk electrode (RRDE) experiments

The catalysts were characterized by CV test at room temperature. The CV curves were obtained by cycling scan after purging N_2 or O_2 for 30 minat a scan rateof 5 $mV.s^{-1}$,.A certain amount of the catalyst was casted onto the pretreated GCE surface with a loading amount of 0.35 $mg.cm^{-2}$. As a comparison, the Pt/C catalyst was prepared

according to the same procedure. RDE measurements were performed with ALS-RRDE 3A Research Instruments. The polarization curves were obtained by performing a negative-direction sweep of potential at a rate of 5 $mV.s^{-1}$ from 1.05 V to 0.3 V (vs. RHE) in 0.1 M KOH or from 1.0 V to 0.2 V in 0.1 M $HClO_4$, and the ring potentials were constant at 1.2 V and 1.5 V vs RHE in 0.1 M $HClO_4$ and 0.1 M KOH respectively. Before experiments, all the electrodes wereactivated by potential cycling in acidic and alkaline media from 1.00 V to 0.10 V for 30 cycles at a scan rateof 50 $mV.s^{-1}$, and the electron transfer number *n*was calculated by the following equation:$n=4*I_d/(I_d+I_r/N)$. Where I_d is disk current, *Ir* is ring current, and *N* is current collection efficiency of the Pt ring. *N* was determined to be 0.39 from the reduction of $K_3Fe(CN)_6$.

c.) Accelerated durability tests in alkaline and acidic media were carried out in O_2 saturated 0.1 M KOH or 0.1 M $HClO_4$ solution with the potential cyclic between 0.5 V and 1.0 V at a scan rate of $50mV.s^{-1}$.

Part B: Tables and Figures

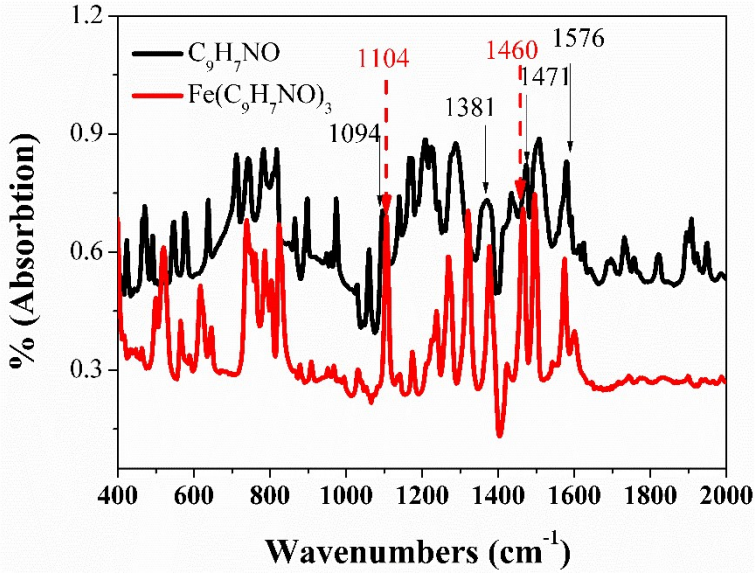

Figure S1: The FT-IR spectra of 8-hydroxyquinoline and8-hydroxyquinoline-iron compounds. (Several feature peaks of 8-hydroxyquinolinemoved in the8-hydroxyquinoline-iron compound, indicative of the formation of the 8-hydroxyquinoline-iron.)

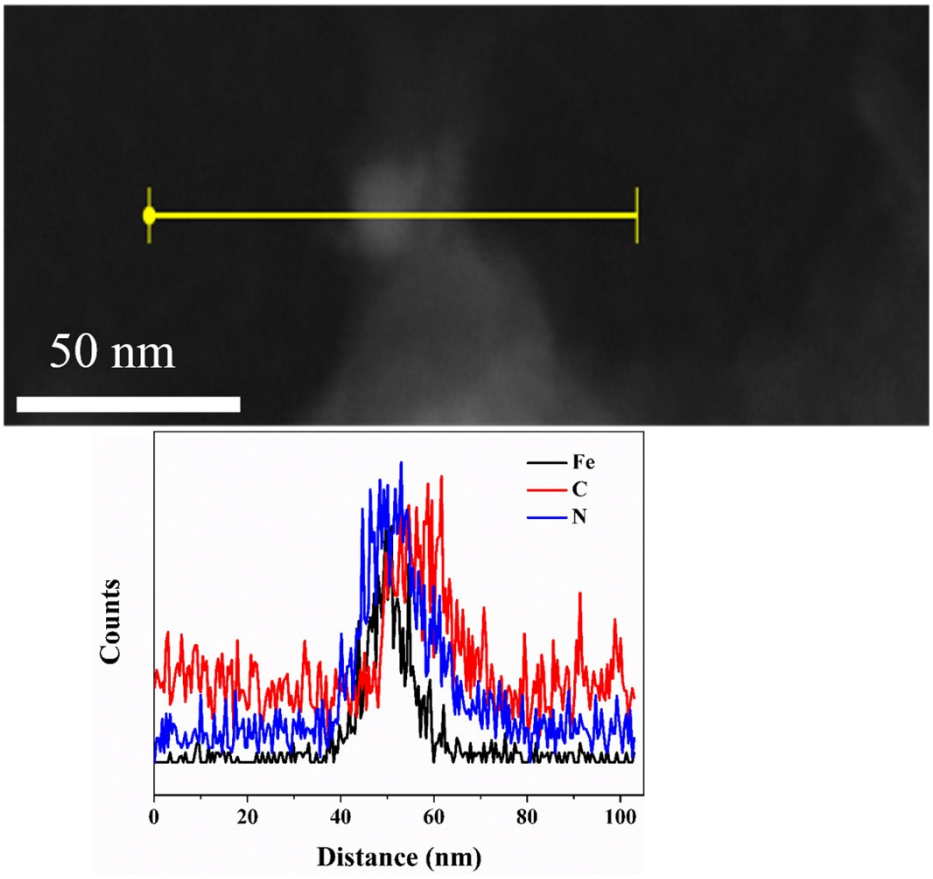

Figure S2.The STEM image and corresponding the line scanning spectrum of the encased iron carbide nanoparticles of 3D-Fe-N-CNS-N

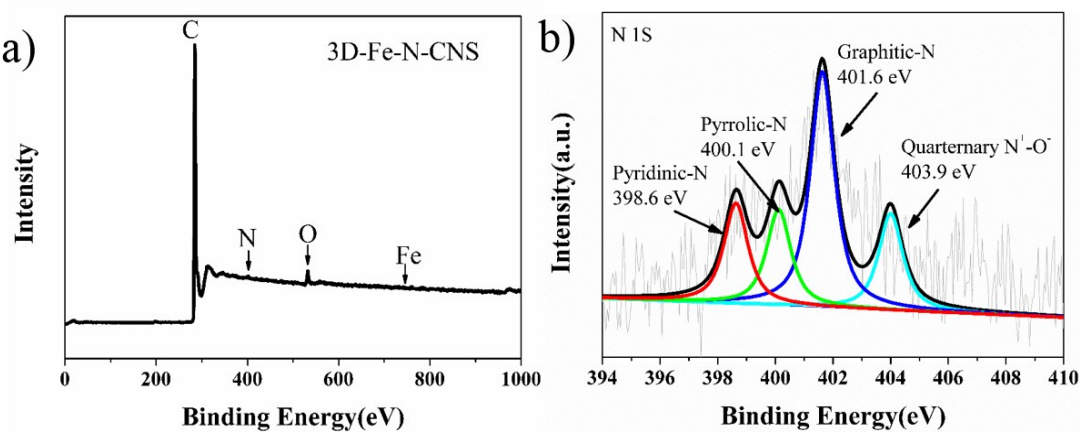

Figure S3: a) The XPS survey spectrum of the 3D-Fe-N-CNS; b) high resolution N 1s spectrum

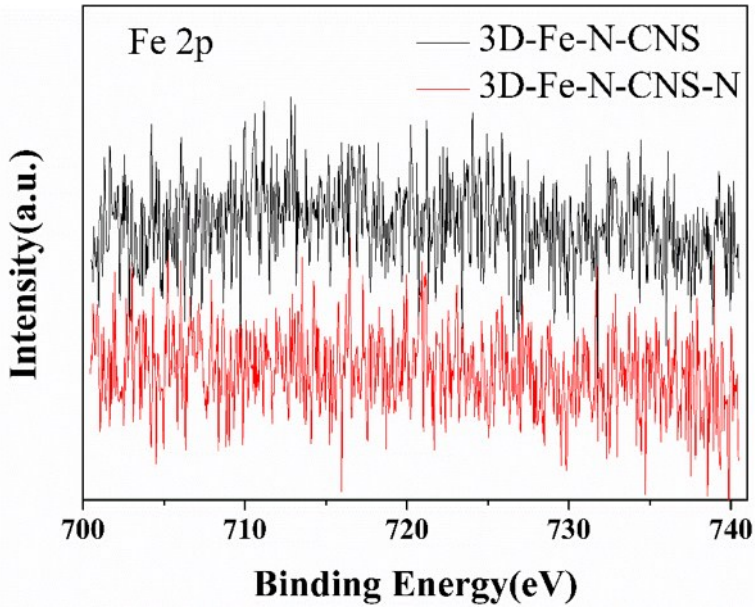

Figure S4.The high resolution Fe 2p spectrum of the 3D-Fe-N-CNS and 3D-Fe-N-CNS

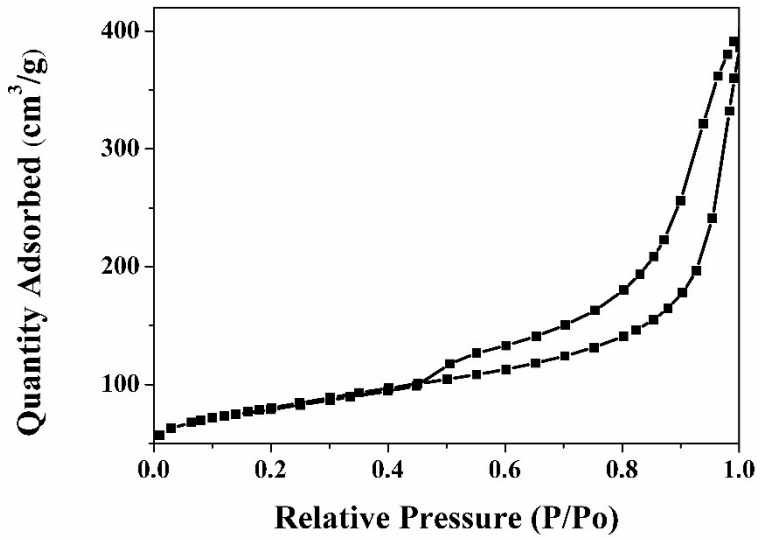

Figure S5. N_2 sorption isotherms of 3D-Fe-N-CNS

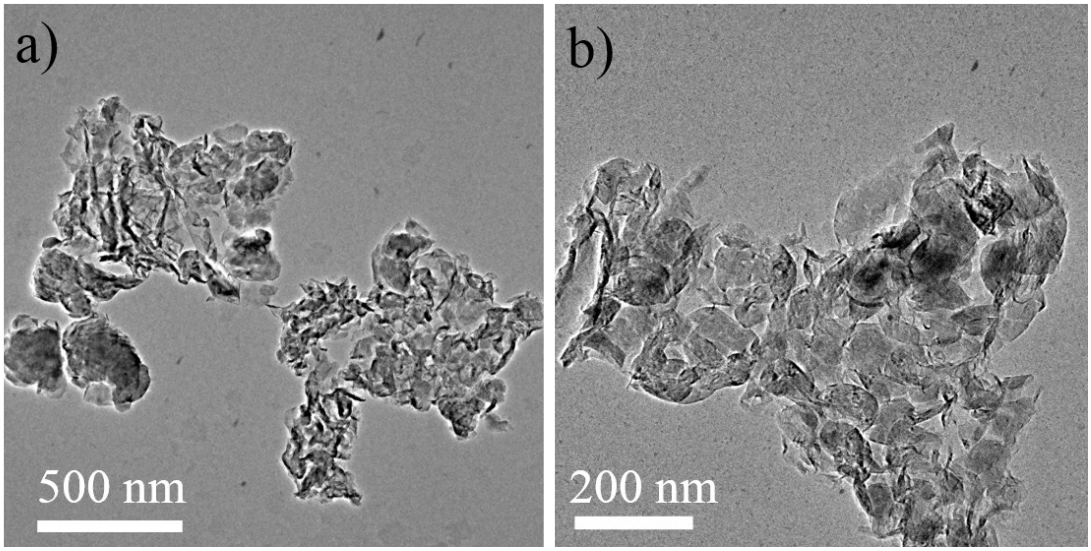

Figure S6.a, b) TEM images of the obtained catalysts before acid etching

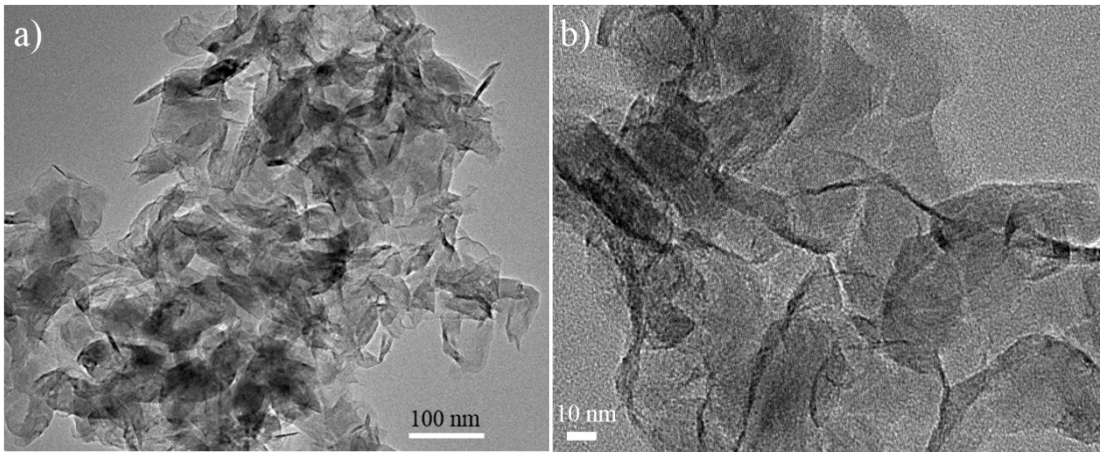

Figure S7.a, b) TEM images of catalyst 3D-Fe-N-CNS

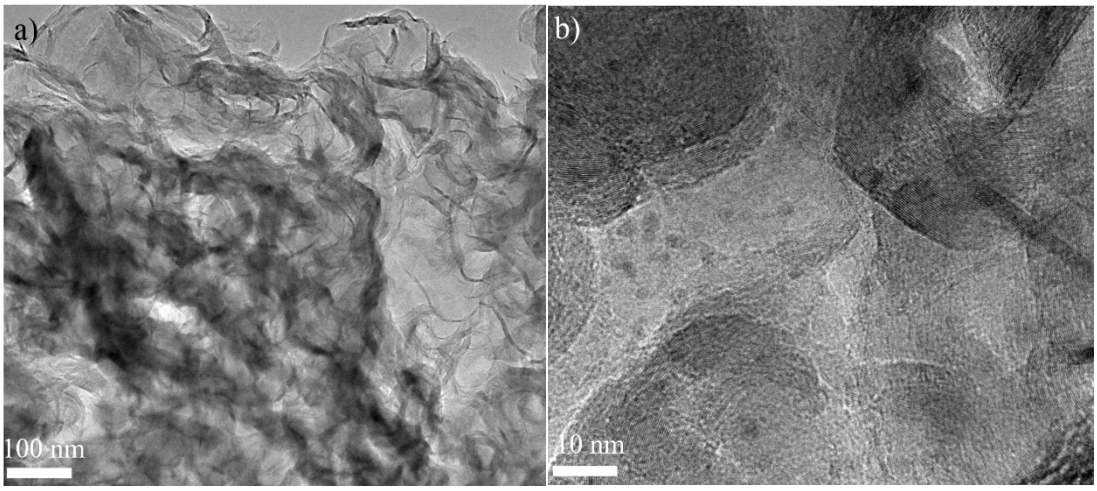

Figure S8.The TEM image of obtained 3D-Fe-N-CNS-N after 4000 cycles in 0.1 M KOH.

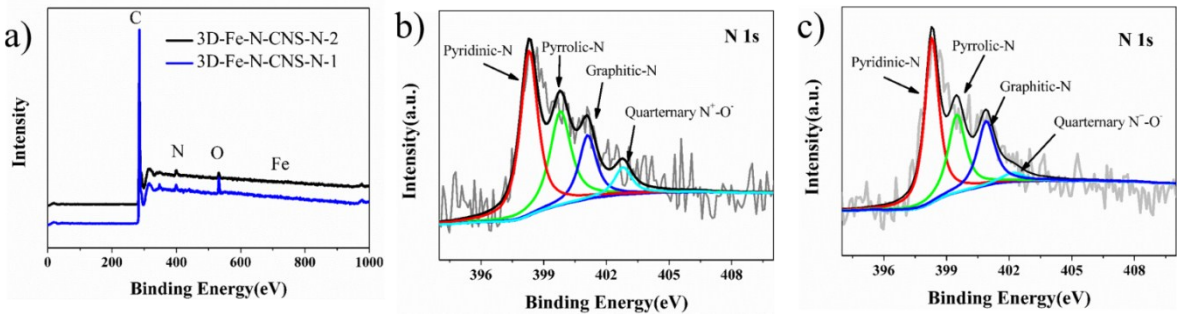

Figure S9.a) The XPS survey spectra of the 3D-Fe-N-CNS-N-1 and 3D-Fe-N-CNS-N-2; b) high resolution N 1s spectrum of 3D-Fe-N-CNS-N-1; c) high resolution N 1s spectrum of 3D-Fe-N-CNS-N-2. (It is noted that the percentum of pyridinic-N in the nitrogen doping of 3D-Fe-N-CNS-N-1 and 3D-Fe-N-CNS-N-2 are 42.8% and 46.2% respectively).

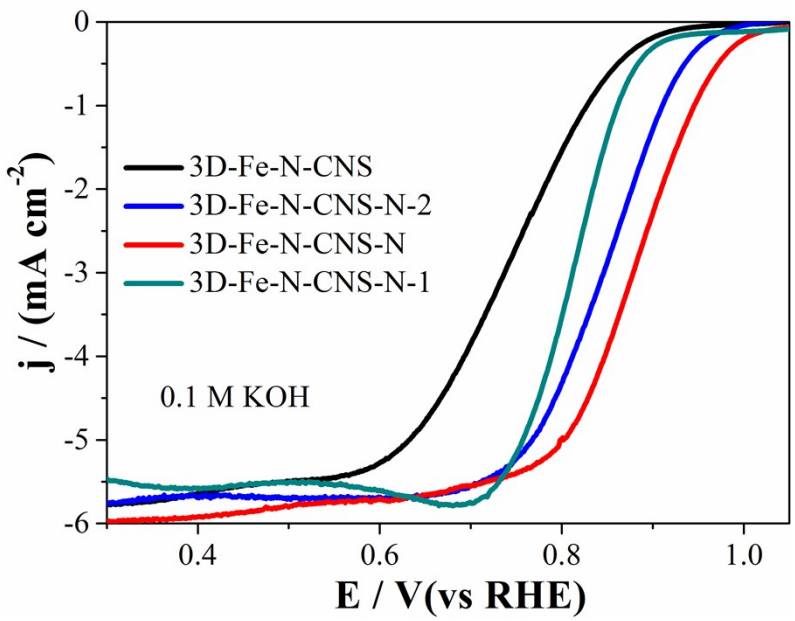

Figure S10.The LSV curves of 3D-Fe-N-CNS, 3D-Fe-N-CNS-N, 3D-Fe-N-CNS-N-1 and 3D-Fe-N-CNS-N-2 with a scan rate of 5 $mV.s^{-1}$.

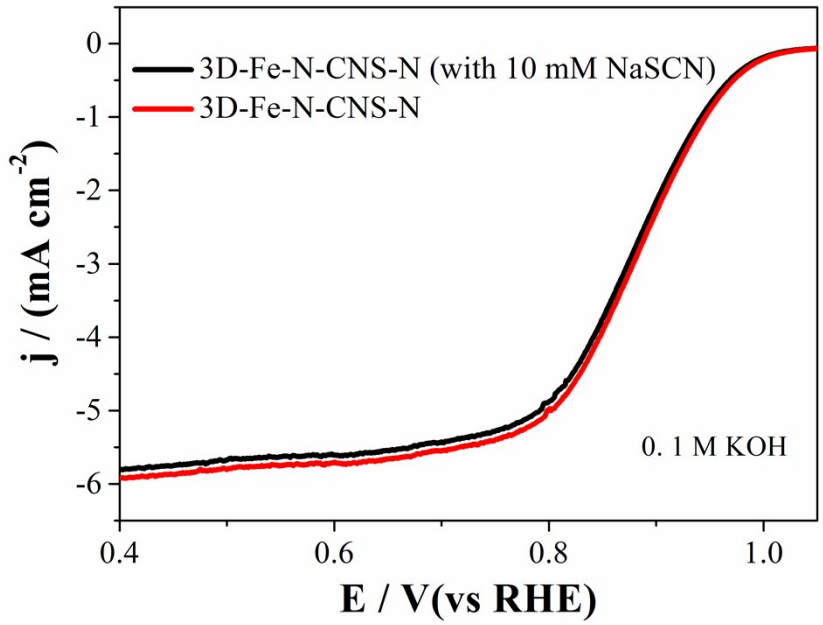

Figure S11. The LSV curves of 3D-Fe-N-CNS-N with/without 10 mM NaSCN in 0.1M KOH

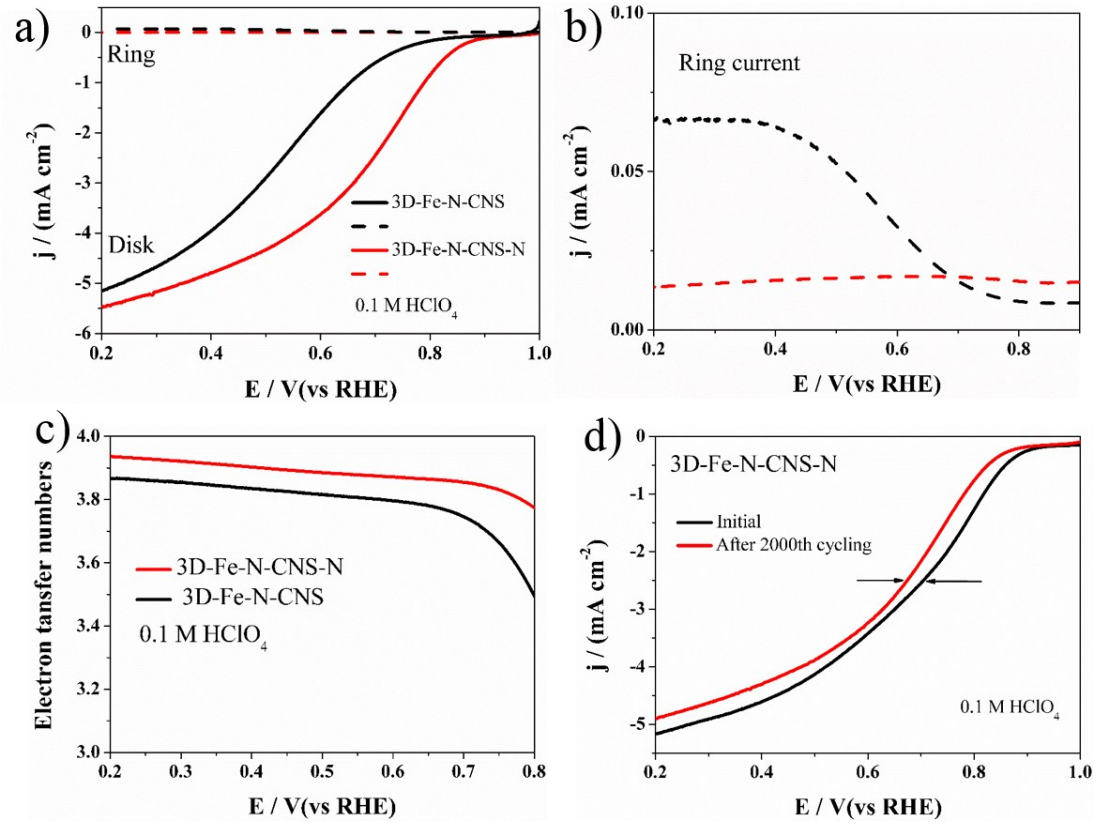

Figure S12.The ORR performance for 3D-Fe-N-CNS-N and 3D-Fe-N-CNS in the acidic medium: a) RRDE curves; b) the Ring current; c) Electron transfer numbers (*n*) of 3D-Fe-N-CNS-N and 3D-Fe-N-CNS; d) The LSV curves of 3D-Fe-N-CNS-N before and after 2000 potential cycles in O_2-saturated 0.1 M $HClO_4$, and the potential was cycled between 0.5 and 1.0 V at a rate of 50 mV.s $^{-1}$.

Table S1.

The content of catalysts measured by XPS

Catalysts	C (at. %)	N (at. %)	O (at. %)	Fe (at. %)
3D-Fe-N-CNS-N	96.01	2.11	1.61	0.34
3D-Fe-N-CNS	96.59	1.05	2.18	0.3
3D-Fe-N-CNS-N-2	94.69	2.03	2.59	0.29
3D-Fe-N-CNS-N-1	96.53	1.31	1.81	0.35

The content of iron for 3D-Fe-N-CNS, 3D-Fe-N-CNS-N-1 and 3D-Fe-N-CNS-N measured by ICP-AES are 2.2 wt %, the cotent of iron in 3D-Fe-N-CNS-N-2 measured by ICP-AES are 2.09 wt %.

Table S2. Comparison of the onset and half-wave potentials(E_{onset}, $E_{1/2}$), number of electrons transferred (n) and corresponding synthetic methods of non-noble metal catalysts stems from literature reprints and this work in alkaline medium

Catalysts	methods	E_{onset} / RHE	$E_{1/2}$ / RHE	Loadings/ ug.cm^{-2}	References
Fe NPs-Carbon nanotubes/NPs	Pyrolyzing carbon supported precursors	--	0.93	1.0	1
P-doped graphene	Doping RGO with phosphorus	0.92	--	--	2
Nanoporous graphene	Doping nanoporous RGO with nitrogen	-0.07 [b]	--	--	3
Meso/microporous nitrogen doped carbon	Polymerizing monomers with monox templates and heating by ammonia	--	0.87	0.5	4
Co_3O_4/N-mrGO	Growing Co_3O_4 on Nitrogen doped RGO	--	0.83	0.1	5
N-doped Fe/Fe3C@C	Pyrolyzing RGO-supported Prussian blue nanoparticles	0.91	0.83	0.78	6
PDMC materials	SBA templates; mesoporous carbon	0.94	--	0.1	7
3D-Fe-N-CNS-N	Hierarchical 3D assembly of crumpled carbon nanosheets	1.03	0.88	0.35	This work

a) RGO: reduced graphene oxide; b) VS. saturated calomel electrode

References

1Active and stable carbon nanotube/nanoparticle composite electrocatalyst for oxygen reduction. *Nat Commun 2013, 4, 1922;*

2Synthesis of phosphorus-doped graphene and its multifunctional applications for oxygen reduction reaction and lithium ion batteries

Adv. Mater. 2013, 25, 4932–4937;

3Nanoporous graphene by quantum dots removal from graphene and its conversion to a potential oxygen reduction electrocatalyst via nitrogen doping.

Energy & Environmental Science, 2014, 7,1059–1067;

4Hierarchically porous carbons with optimized nitrogen doping as highly active electrocatalysts for oxygen reduction.

Nature Communications 2014, 5, 4973-4973;

5Co_3O_4 nanocrystals on graphene as a synergistic catalyst for oxygen reduction reaction.

Nature Materials 2011, 10, 780-786;

*6*Metal−organic−framework derived nitrogen‐doped core‐shell‐structured porous Fe/Fe3C@C nanoboxes supported on graphene sheets for efficient oxygen reduction reactions.

Advanced Energy Materials (2014);

7Efficient metal-free electrocatalysts for oxygen reduction: polyaniline-derived N- and O‑Doped mesoporous Carbons. *J. Am. Chem. Soc. 2013, 135, 7823−7826;*